npj | heritage science

Article

https://doi.org/10.1038/s40494-026-02339-4

Integrated portable spectroscopy for the analysis of Roman mosaics from Marroquíes Altos, Jaén, Spain

Alberto Sánchez[1] ✉, Manuel Montejo[1,2], José Tuñón[1], Peter Vandenabeele[3], Pieter Tack[4], Sara Valadas[5] & Teresa Reis[5]

This study presents an integrated archaeometric analysis of three key Roman mosaics (Tethys, Erotes, and Scrollworks) from the Marroquíes Altos site (Jaén, Spain), currently displayed at the Museum of Jaén. The aim was to enhance their historical value and define their regional features within the Upper Guadalquivir Valley. The innovative, non-destructive methodology integrated systematic photogrammetric digitization with portable spectroscopic techniques (handheld Raman and h-XRF), which was essential as the mosaics are wall-mounted. A large dataset was generated and processed using multivariate statistical analysis (PCA). Results confirmed the use of locally sourced limestone but, crucially, identified the widespread presence and selective use of ironstone (haematite) across two of the three mosaics. This unique finding strongly supports the existence of a distinctive regional practice within the Roman mosaic school of Jaén, setting the local production apart from other Roman mosaics in Europe and advancing a comprehensive understanding of the region's material culture.

Roman presence in the so-called Upper Guadalquivir Valley (current province of Jaén, Andalusia, Spain) is documented from the late 3rd century BC to the 5th century AD. Over these centuries, a process of Romanization gradually unfolded, leading to profound transformations in the social, economic, cultural, and territorial organization of the pre-existing Iberian societies. Consequently, the province of Jaén preserves a rich and valuable archaeological heritage from the Roman era. Significant finds include evidence of military actions like the Battle of Baécula[1], as well as major urban centers such as Cástulo, Obulco, Tucci, Isturgi, and Iliturgi[2]. Other notable discoveries comprise monuments like the arch of Ianus Augustus[3], sections of the Via Augusta[4], and large rural residential complexes known as *villae*. As ornamental elements within these structures, important and spectacular mosaics -exhibiting high levels of technical and iconographic complexity- have been preserved. Although commonly used as pavements in various kinds of buildings -civil, religious, commercial, and thermal- they were most prevalent in private residences.

Many of these mosaics, dating from the 1st to the 5th century AD, are currently preserved and displayed on the walls of museums or in situ on the floors of archaeological sites in Jaén. Despite their undeniable interest, the information available for their valorisation still has considerable potential for further development. In this context, the GeoChemMos project was launched in 2023, aiming to carry out an archaeometric, multidisciplinary and systematic study of this corpus of mosaics with spectroscopic techniques, specifically hand-held Raman (h-Raman) and X-Ray fluorescence spectroscopies (h-XRF), playing a central role. The effectiveness and utility of these techniques in mosaic analysis have been demonstrated through their widespread application at prominent heritage sites over the past quarter-century. Numerous studies of tesserae have been undertaken to identify the raw materials (types of stone, glass, pottery, etc.) and establish their provenance, determine the manufacturing techniques, identify production workshops, chronologically reclassify the mosaics and analyse deterioration processes[5–16].

All six Roman mosaics currently displayed at the Museo Provincial de Jaén form part of the GeoChemMos project. Among them, three from the Marroquíes Altos archaeological site are of special interest: namely the Tethys, Erotes, and Scrollworks mosaics. They were discovered in 1959 during the excavation of a Chalcolithic cave with funerary use in the urban area of the city of Jaén (Supplementary Fig. 1). Above this cave appeared a series of ashlar blocks linked to a Roman building with an apsidal plan to which the mosaics would have belonged[17]. Although descriptive and iconographic aspects have been made public in some published works[18–20], the archaeological information and context of the mosaics have been lost or

[1]University Research Institute for Iberian Archaeology, University of Jaén, Campus Las Lagunillas, Jaén, Spain. [2]Department of Physical and Analytical Chemistry. University of Jaén, Campus Las Lagunillas, Jaén, Spain. [3]Department of Archaeology, University of Ghent, Ghent, Belgium. [4]Ghent University Centre for X-ray Tomography (UGCT), Department of Physics and Astronomy, Ghent University, Ghent, Belgium. [5]HERCULES Laboratory, University of Évora, Évora, Portugal. ✉e-mail: vizcaino@ujaen.es

Fig. 1 | Up: Mosaic of Tethis. Lower left: Erotes Mosaics. Lower right: Scrollworks Mosaic.

were never published. Consequently, little to nothing is known about their archaeological context, the nature and origin of the raw materials used, or the restorations carried out on them. The only mosaic on the set for which spectroscopic data about stone tesserae are available is the Tethys mosaic, and this information has been retrieved and expanded upon in this work[21].

In this study, the three aforementioned mosaics have been subjected to thorough research from both archaeological and methodological perspectives. Archaeologically, the aim was to enhance their value as historical documents, enabling interpretations that extend beyond purely aesthetic considerations. This required generating new interpretative data to characterize the raw materials employed in their manufacture. Methodologically, the study faced several challenges due to the high number of samples potentially available for analysis and the absence of loose tesserae. Accordingly, key aspects -optimizing the sampling strategy, jointly interpreting data obtained from two complementary portable spectroscopic techniques, and handling large volumes of experimental data- were systematically addressed.

The first of the mosaics studied, the Tethys Mosaic, is a polychrome semicircular mosaic (Fig. 1, up) that features Tethys, a Titaness of the sea in Greco-Roman mythology who personifies the moisture that makes everything germinate. She is the daughter of Uranus and Gaia, sister and assistant of Oceanus, and mother of all rivers and the three thousand Oceanids[22]. The mosaic, dated to the second half of the 4th century AD, is semicircular and likely belonged to an exedra in a prestigious room such as the *oecus*, or perhaps adorned a fountain.

The bust of Tethys is shown with a wing or fin on the back of her head and crab legs on either side of her forehead. A snake-like fish coils around her neck like a necklace. Her figure appears between two khetoi (sea monsters) that gaze toward her, while a paddle is depicted to her left. Around her, dolphins, fish and a shell complete the marine imagery. The mosaic was restored and most likely rebuilt in its right section from the paddle onward. Its present dimensions are 1.80 m in height and 4.70 m in width[18,19].

The second mosaic, the Erotes Mosaic, is a polychrome mosaic (Fig. 1, lower left) that follows the well-known Roman *compass* scheme: a central circle surrounded by four tangent semicircles and four quarter circles in the corners, all inscribed within a square[18]. Two figures representing *erotes* (cupids in Roman mythology) are fundamentally preserved. The first, in the lower semicircle (bottom right), appears to be rowing a small boat, with the sea rendered in lines of blue tesserae. The second, partially preserved in the central rhombus, is depicted in flight.

In the preserved part of the central circle (upper section), only a marine setting with lines simulating the sea is visible, along with what may be another *erote* and possible rock formations. The circles and semicircles are framed with interlaced or knotted polychrome motifs. The mosaic measures 1.73 m in height and 1.87 m in width. It has been dated to the 4th century AD, although some authors suggest an earlier chronology, i.e., the 2nd century AD[23].

Finally, the third mosaic is known as the Scrollworks Mosaic. Only a corner of this mosaic, dated to the 2nd century AD, has been preserved (Fig. 1, lower right). The outer area is decorated with three spiral scrollworks with leaves set against a white background, where several white Maltese crosses are also visible. Inside, an angle delimited by a black line can be seen, containing two polychrome cable motifs, the second of which is only partially preserved. The surviving dimensions are 1.44 m in height and 1.68 m in width[19].

Methods

Digitization

Each mosaic was digitized using photogrammetry under controlled, uniform lighting conditions to improve the system for selecting and locating tesserae for analysis by h-Raman and h-XRF, as well as to facilitate the dissemination of the results. This approach was adopted due to the variable lighting conditions at the locations where the mosaics are displayed, which could otherwise affect the sampling process. In total, 3046 photographs were taken (1816 of Tethys, 696 of Erotes, and 534 of Scrollworks).

The digitalization process was carried out using Agisoft Metashape, which enabled the alignment of each photo set and the generation of a sparse point cloud for every mosaic. A dense cloud was then created to produce a polygon mesh, to which a photo-derived texture was applied, resulting in a detailed 3D model. The exported orthophotos reached sizes of up to 187,406 × 79,260 pixels, with a resolution of 0.404 mm/pixel. Subsequently, Adobe Photoshop was used to enhance the orthophoto's sharpness through an unsharp mask, and to improve brightness and contrast by approximately 30%. (Supplementary Figure 2).

Given the high resolution of the orthophotos, the three mosaics are easily viewable and accessible via GigaMacro Viewer: Tethys Mosaic, Erotes Mosaic, and Scrollworks Mosaic.

Selection of measured tesserae

For this task process, the use of the orthophotos proved crucial, as their high resolution allowed for precise observation of the tesserae without the need to be physically present at the museum where the mosaics are displayed, thus avoiding the potential influence of variable lighting conditions on the decision-making process. The tesserae selected for analysis were chosen to ensure adequate representation of all types, with the types primarily defined based on colour and texture, and with particular attention to their state of conservation, which also served as discriminating factor. In this way, 27 types were identified in the Tethys mosaic, 23 types in the Erotes mosaic, and 9 types in the Scrollworks mosaic (Fig. 2). From each type, 5 tesserae were selected, resulting in a total of 306 tesserae (Supplementary Figs. 3–5, Supplementary Table 1).

In some cases, the number of available tesserae of the same type, or the state of conservation of the tesserae belonging to a given type, did not allow for the selection of five individuals for analysis. In such instances, the number of tesserae selected was consequently reduced. In other cases, after a more detailed visual analysis, several types were reunited into a single one, which increased the number of tesserae of that type, which were nevertheless analysed to confirm the homogeneity of that type.

All selected tesserae were analyzed with h-Raman. Choosing five specimens per type introduced redundancy, which allowed those that failed to yield a clear signal to be disregarded without compromising representativeness. In this context, representativeness refers not only to the sufficient number of tesserae examined but also to the reliability with which the composition of each type was established. As concerns h-XRF, only 3 of the 5 tesserae selected per type were analysed. This decision was based on two factors: first, the time required for h-XRF measurements was considerably greater than for h-Raman; and second, h-XRF consistently yields a clear signal, making three measurements sufficient to obtain accurate elemental composition data while balancing efficiency and the reliability of the results. Consequently, 284 tesseare were measured by h-Raman and 174 by h-XRF.

Handheld Raman Spectroscopy (h-Raman)

For the Raman analyses, a portable BWS445-785S innoRam™ Raman spectrometer (BWTEK, Inc., Newark, USA) was used. This equipment, featuring a 785 nm excitation laser with a maximum power of 300 mW, offered an approximate spectral resolution of ~ 4 cm^{-1}. It incorporated a TE-cooled, back-thinned, 2D binning CCD detector. The tesserae were measured using a 1.5-metre fibre optic probe, manually focused. The lens used had a 5.9 mm working distance regulator, which allowed for precise focusing while minimizing contamination and degradation of the lens material. The spot size was 85 µm. To ensure an adequate signal-to-noise (S/N) ratio, low laser power was maintained, and the measurement time and accumulations were adjusted. No special calibration was applied. Before each measurement, a dark scan was performed to improve the S/N ratio in the Raman spectra. Experimental conditions varied: exposure time ranged from 100 to 1000 ms, maximum power was 100%, with a maximum of 60 acquisitions, and a spectral range between 65 and 3000 cm^{-1}. The equipment was powered by both a Pb-ion battery (MICROBEAM S.A., Barcelona, Spain) and a portable generator. Raman spectra acquisition was managed using BWSpecTM software, version 3.26 (B&W Tek Inc.).

As aforementioned, Raman spectroscopy is a well-established technique that provides exceptional structural sensitivity, is fast, respects the integrity of archaeological material and is widely employed in heritage studies. Nonetheless, certain limitations must be acknowledged: the reduced spectral resolution of bands from non-crystalline mineral compounds, fluorescence interference (particularly affecting glass samples), and the generally lower sensitivity and spatial resolution of portable instruments compared to benchtop systems[24,25]. These circumstances highlight the importance of a complementary analytical strategy.

Handheld X-ray fluorescence (h-XRF)

The in-situ analyses were performed with an Olympus Innov X Delta Premium commercial instrument coupled with a rhodium (Rh) anode-based X-ray tube and a 20-mm^2 silicon drift detector (SDD). An aluminium (Al) filter was applied for measuring the higher Z-elements (from Fe onwards) with a voltage of 40 kV and a current of 38.7 µA. Without filtering (low-Z elements), a voltage of 10 kV and a current of 50.8 µA can be applied. The measurements were performed in air for 150 s (live time) with the Geochem mode of the instrument. All measurements were performed with a collimated polychromatic X-ray beam for excitation (3×3 mm^2). This equipment also had a camera that allowed the correct positioning of the instrument and viewing of the analysed area.

To ensure calibration and allow for the calculation of element concentrations, the data were processed using the dedicated XRF spectrum evaluation software PyMca5[26]. The XRF results were quantified using references NIST 2710a, NIST 98b, NIST 2711a, NIST 610, NIST 612, NIST SRM 611, and NIST 679 based quantification method. The XRF elemental yield was determined for each certified element in the reference materials by dividing the XRF net peak intensity by the corresponding certified concentration. Where an element is present in multiple reference materials, the average elemental yield and its standard deviation were used as a resulting error. For elements that are not present in any of the used reference materials, the elemental yield was estimated by interpolation of the closest neighbouring elements, by atomic number and XRF line type, which were present in the reference materials. The XRF intensities were normalised for measurement time preceding elemental yield calculation. The quantification model assumed an average density of 4.25 g/cm^3 and a maximal thickness of 1.5 cm for the unknown samples.

Despite its utility and advantages (speed, efficiency, versatility, non-destructive character, good precision and accuracy), h-XRF analysis still faces several limitations when applied to archaeological materials like stone or glass. These drawbacks primarily involve a difficulty in providing accurate data for light elements (those with an atomic number $Z < 14$), and limited accuracy in quantifying some elements due to the overlapping of specific fluorescence lines. Furthermore, matrix effects must always be taken into consideration[27,28].

Data analysis

In this study, the structural insights provided by h-Raman (Supplementary Table 2) were integrated with the elemental composition information obtained from h-XRF. As concerns the latter, the analysis of the tesserae from the three mosaics (174 in total) produced a large and complex dataset (Supplementary Tables 3-5) that required the implementation of multivariate analysis to extract relevant information and group the tesserae types based on their composition. Accordingly, PCA analyses were applied to different subsets of the dataset: (1) all tesserae, (2) stone tesserae, and (3) glass tesserae. This strategy enabled a direct comparison among the three mosaics, facilitated the detection of groups based on elemental composition similarities, and provided more stable results with reduced noise by considering a larger number of individuals.

h-XRF data analysis was performed with a Python script developed ad hoc. The workflow included data cleaning, normalization, optional logarithmic transformation, and standardization. Principal Component Analyses (PCA) were conducted using the scikit-learn implementation, which

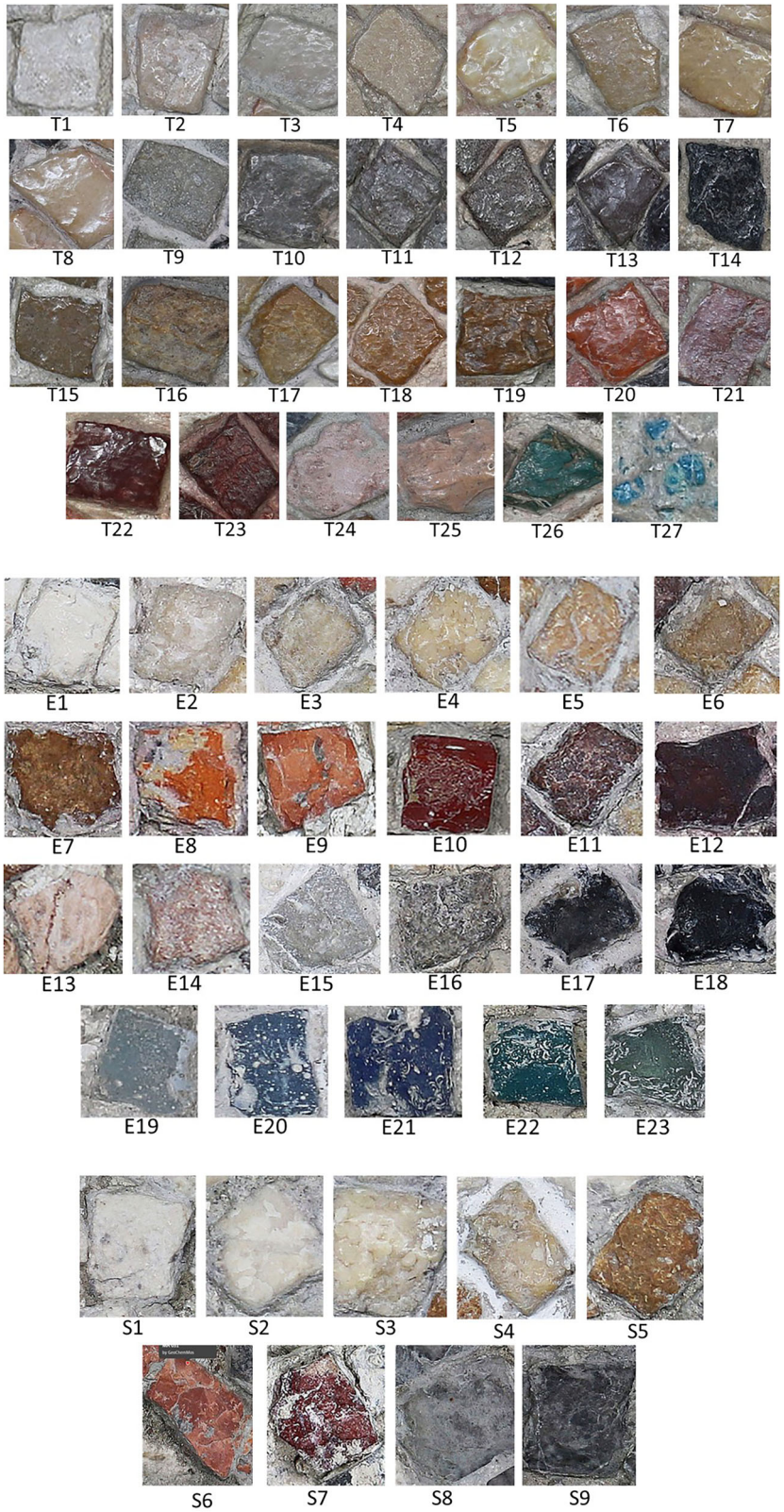

Fig. 2 | Types of tesserae. T: Tethys. E: Erotes. S: Scrollworks. Tesserae size range between 7 and 13 mm.

applies a Singular Value Decomposition (SVD) to the standardized data matrix, ensuring reproducibility and the extraction of components that maximize explained variance. The script also generates biplots and graphical visualizations to support data interpretation and can be executed in environments such as Google Colab, Jupyter Notebook, or any Python-compatible IDE.

Results

For the PCA of all tesserae, eleven elements commonly selected in joint studies of stone and glass (Al, Si, K, Ca, Ti, Mn, Fe, Sr, Cu, Sb, and Pb) were considered, with a $\log_{10}$ transformation applied to balance differences in relative signal intensity[28]. PC1 and PC2 together explained 69.2% of the variance. The results show a clear separation between stone and glass

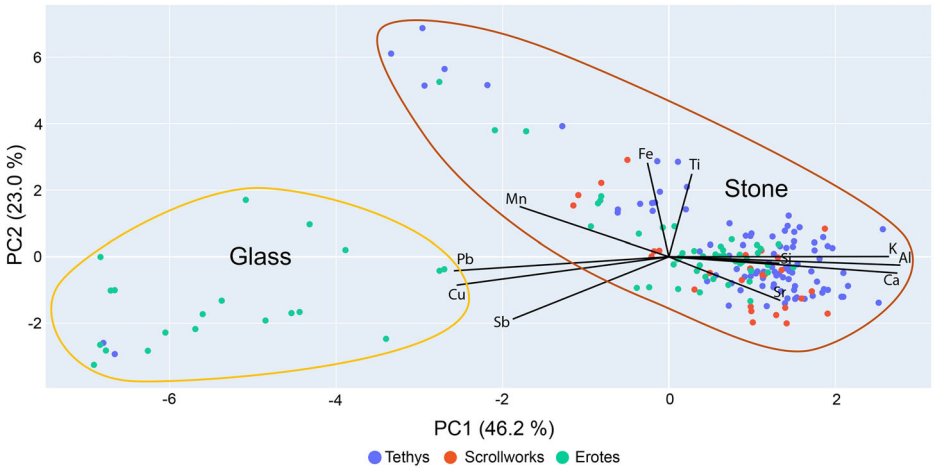

Fig. 3 | PCA results based on h-XRF data (after log10 transformation) from all tesserae under study.

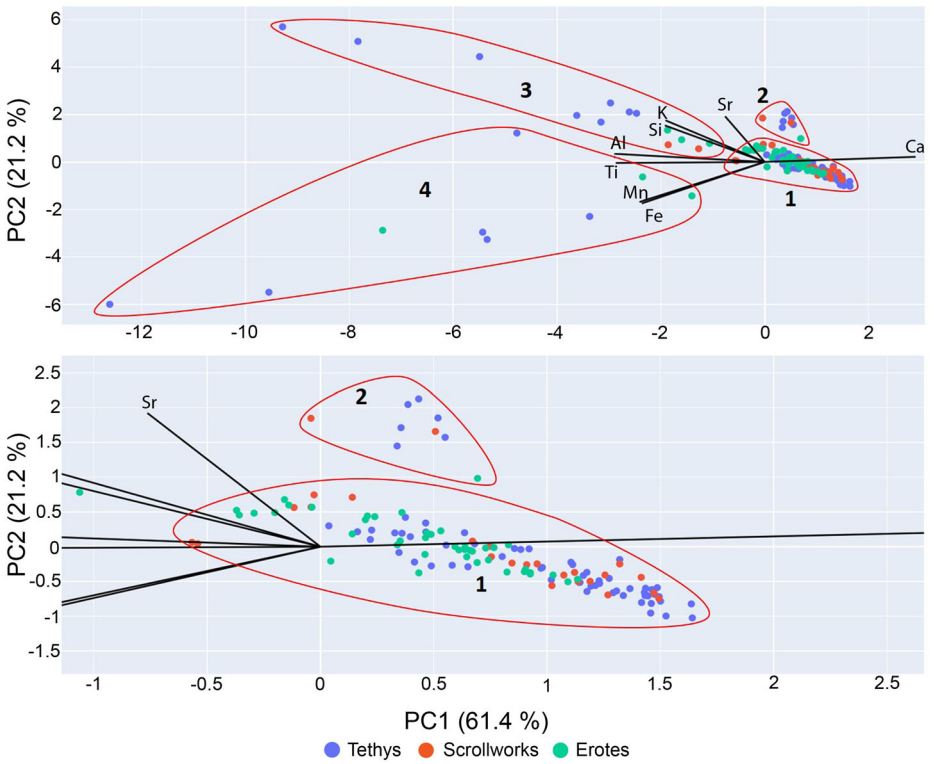

Fig. 4 | Up: PCA results based on h-XRF data from all the stone tesserae. Down: A magnified view of the clusters corresponding to groups 1 and 2.

tesserae, the latter representing the minority (Fig. 3). With the exception of two tesserae (102 and 103) from the Tethys mosaic, all glass tesserae were used in the Erotes mosaic.

Stone tesserae

For the subset of stone tesserae (n = 152), a second PCA was performed using the eight elements most typically considered in lithic characterization (Al, Si, K, Ca, Ti, Mn, Fe, and Sr). In this case, PC1 and PC2 accounted for 82.6% of the variance. As shown in Fig. 4, the PCA allowed the definition of four compositional groups among the stone tesserae. Group 1 comprises tesserae whose composition is dominated by Ca; Group 2, those whose composition is dominated by Ca but is enriched in Sr; Group 3, tesserae whose composition shows lower Ca and a variable but notable presence of Si; and Group 4, tesserae whose composition is enriched in Fe.

Limestone tesserae. Among the large number of stone tesserae analysed, the vast majority fall within the so-called groups 1, 2 and 3. They were identified as limestones as a result of the Raman spectra obtained, which exhibited the diagnostic calcite bands at ~1085 cm^{-1} (symmetric stretching mode of the carbonate ion), ~712 cm^{-1} (in-plane bending mode), and below 300 cm^{-1} (~157 and ~283 cm^{-1}), corresponding to translational and rotational lattice modes[29–31] (Supplementary Table 2). The observed differences in spectral intensity and resolution among these tesserae may be related to surface irregularities, state of preservation, or structural factors such as crystal orientation and particle size[32,33]. These parameters can influence overall spectral quality and are difficult to control given the limited spatial resolution of the fibre-optic probe and the small size of the tesserae, which restricts the possibility of exploring alternative measurement points to obtain better spectra. Additionally, in some cases, the presence of consolidants applied during restoration may increase fluorescence background and reduce the signal-to-noise ratio.

In some tesserae, specifically the black/gray ones (see Fig. 2; Erotes Mosaic, type E17; Scrollworks Mosaic, type S9), known as *bigi morati*, the Raman spectra also revealed the presence of amorphous carbon derived

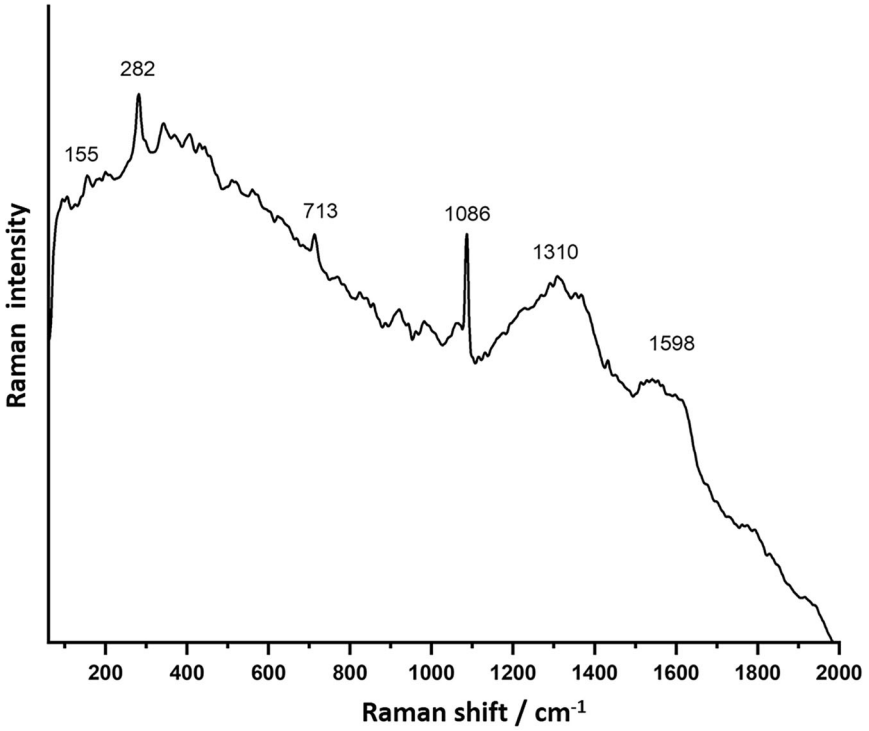

Fig. 5 | Erotes Mosaic. Tessera 9, type E17. Raman spectrum of calcite and amorphous carbon. (Experimental conditions: 785 nm, 300 mW, 600 ms/acc, 40 accumulations).

from organic material, responsible for their dark coloration. This is evidenced by the presence of the characteristic D band (1300–1350 cm^{-1}) and G band (1550–1600 cm^{-1}) typical of amorphous carbon (Fig. 5)[34,35].

While Raman spectroscopy suggests an apparent compositional uniformity among the different types of limestone tesserae in the three mosaics, belonging to the so-called groups 1, 2 and 3, XRF data reveal distinct variations in the elemental composition of the raw materials. In order to further investigate these variations, the composition of these tesserae were examined in detail through binary plots comprising pairs of elements with discriminatory potential.

In the case of the so-called Group 1 of stone tesserae, the PCA already reveals a differential clustering between samples from the Tethys and Erotes mosaics (Fig. 4). A bivariate analysis of Ca versus Si provides additional insight into this compositional variability (Fig. 6). Tesserae from both mosaics are clearly Ca-dominated, with Ca representing the major constituent relative to Si. However, the Erotes tesserae show a slight Si enrichment compared to those from Tethys. The Scrollworks mosaic displays a more heterogeneous elemental pattern, without a consistent correspondence with either of the two preceding trends.

In the PCA results (Fig. 4), Group 2 is already distinguished from the other tesserae clusters. This group comprises black to dark-gray limestone tesserae, and the bivariate analysis of Ca versus Sr (Fig. 7) highlights their higher Sr levels as the main compositional feature distinguishing these samples. Tesserae belonging to this group occur in all three mosaics, although the Tethys mosaic is overrepresented due to the larger number of samples analyzed from this context. Additionally, three gray tesserae from the Tethys mosaic (122, 123, and 124, type T10) display intermediate Sr values but, owing to their higher Si contents, appear to be more closely related to Group 3.

As regards Group 3, it comprises gray, yellow and brown tesserae characterized by lower Ca levels and an overall enrichment in Si and, to a lesser extent, in K, Al and Ti. These tesserae are particularly associated with the figure of Thetys, Ketos and the shell motif in the Tethys mosaic. They also occur in the knotted cords of the Erotes mosaic and in one of the scrolls of the Scrollworks mosaic.

A striking subset of the tesserae are three specimens (122, 123, 124, type T10) from the Tethys mosaic, located at the contour of the deity's face and ear. These specific tesserae exhibit a remarkably high concentration of Si, Al, and K, accompanied by measurable quantities of Ti and Fe. The elements Si, Al, and K constitute the principal components of numerous clay minerals (such as kaolinite or illite), which are fundamentally aluminium silicates. The presence of Fe and, to a lesser extent, Ti, is consistently observed as trace elements or impurities within these argillaceous minerals or associated oxides/hydroxides. Consequently, it is inferred that the non-carbonate fraction of these tesserae is primarily composed of argillaceous material, thereby validating the proposal of marly limestone as raw material for their fabrication.

The extensive use of limestone in the three mosaics is closely linked to its abundance in the area surrounding the city of Jaén, which lies at the foot of several mountain ranges belonging to the Baetic System. The nearest of these is the Sierra Sur, composed mainly of Cretaceous and Jurassic limestones containing calcite marine fossils and occasionally exhibiting oolitic or reddish textures[36]. Limestone quarries have been continuously opened and exploited in this range up to modern times (Supplementary Figure 6). In addition to its abundance, this material offers several properties that make it particularly suitable for mosaic production: ease of cutting and polishing, compact texture, low porosity, and uniform coloration[37].

Ironstone tesserae. Within the analysed rock tesserae, Raman data indicate a markedly different composition compared with the limestone tesserae, corresponding to a distinctive set of dark red samples identified as types T22, T23, E12, and S7 (Fig. 1). Their Raman spectra (Fig. 8) repeatedly display well-defined bands at 226, 293, 412, and 611 cm^{-1}, which can be unambiguously assigned to the characteristic vibrational modes of haematite[38–40].

Notably, this set of samples coincides with Group 4 as defined by the XRF results. This group comprises tesserae characterized by high Fe levels. Along with the presence of haematite, this result confirms the use of ironstone as the raw material for their production. The Fe content in iron ores is known to vary widely (reaching up to about 70 wt% in the purest forms) and is typically accompanied by variable amounts of Si, Ti, Al, P, S, and Mn[41,42]. This compositional variability accounts for the broad range and dispersion observed among tesserae within this group.

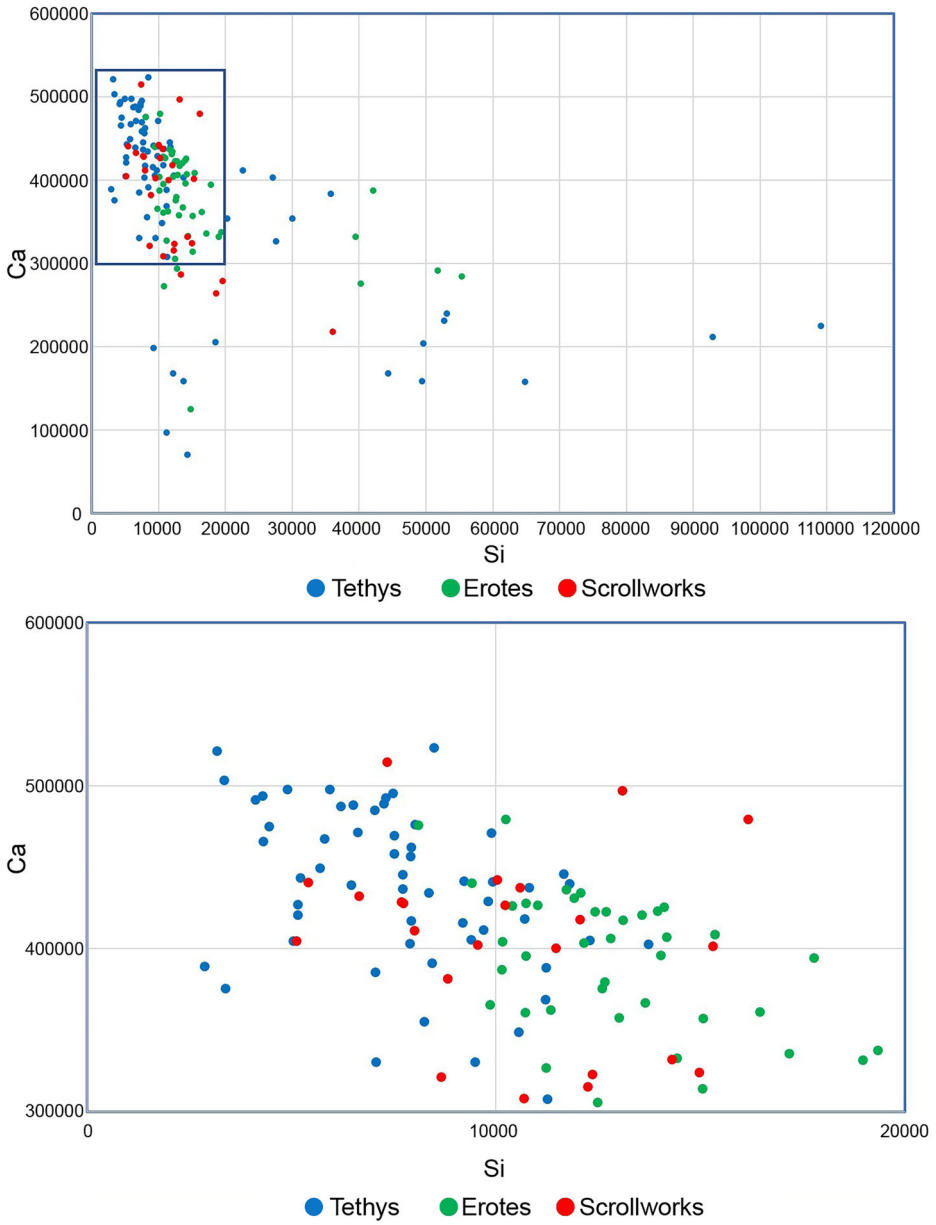

Fig. 6 | Up: Bivariate plots of Si (ppm) versus Ca (ppm) for stone tesserae . Down: A magnified view of the area in the inset.

It is worth noting that the presence of Fe in the red tesserae from the Scrollworks mosaic (38, 39, 40; type S7) is evidenced by their recurrent exhibition of a Raman spectrum consistent with haematite (Fig. 8D), a result that may be influenced by the limited spatial resolution associated with the use of a macroscopic Raman probe. Nonetheless, the relative abundance of Fe in this set, together with additional compositional particularities, does not warrant their inclusion in Group 4. For this reason, these tesserae should instead be regarded as specimens manufactured from iron-rich limestone.

Although iron ore outcrops, exploited up to the 20th century, are well documented throughout the province of Jaén and are particularly abundant in the vicinity of the Marroquíes Altos site[36,43] (Supplementary Figure 6), the reasons behind the selection of ironstone for the mosaics of Jaén remain a question that requires further research.

Beyond this local availability, other characteristics may have justified its selection on both technical and aesthetic grounds. For example, the hardness of haematite, the principal mineral in ironstone (5–6 on the Mohs scale), allows it to be worked with cutting tools and polished, while its intense dark red colour clearly distinguishes it from the lighter red tones of limestone or sandstone. Further virtues attributed to haematite were already highlighted in classical sources by Pliny the Elder in *Naturalis Historia* and by Dioscorides in *De Materia Medica*, who praised it for its medicinal properties, its believed power to protect against blood diseases, and its use as an amulet for courage. These combined factors could help explain its appeal to local artisans, although the question remains as to why this material appears to have been rarely, if ever, employed in other regions of the Roman Empire.

From a decorative standpoint, the use of ironstone tesserae also appears to have followed deliberate aesthetic criteria. In the Tethys mosaic, these tesserae were employed selectively in the depiction of the goddess's hair, antennae, and oar, as well as in all the fish. In the Erotes mosaic, they appear in the figures of the Erotes and in the boat.

Glass tesserae

Although the group of glass tesserae analysed is limited in number, it displays a notable chromatic diversity, including black, orange, red, blue, and green tones. In the Erotes mosaic, they are used for the decoration of the boat, in the lines that represent the sea, and especially in the two erotes. In the Tethys mosaic, they have only been preserved and identified in the eye of the dolphin and in the right eye of Tethys.

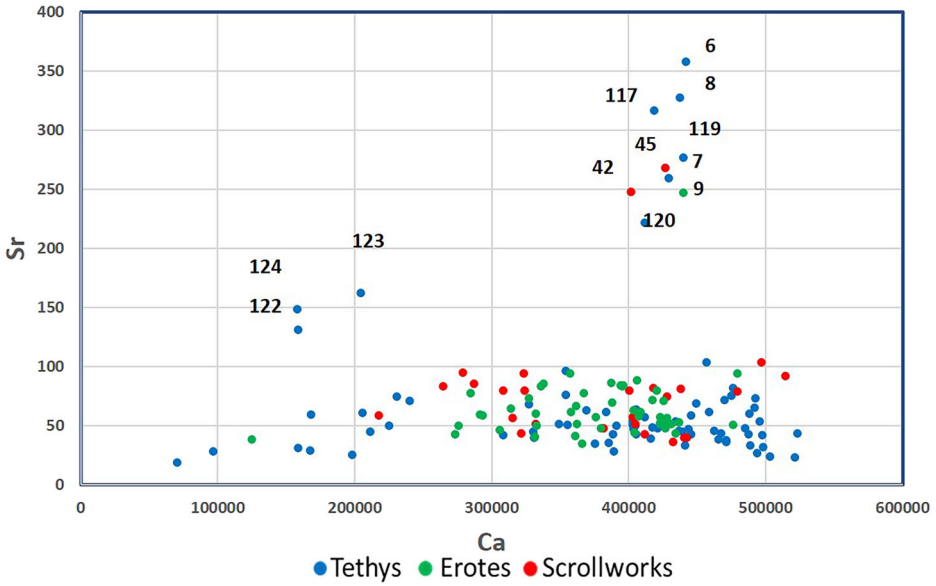

Fig. 7 | Bivariate plot of Ca (ppm) versus Sr (ppm) for stone tesserae.

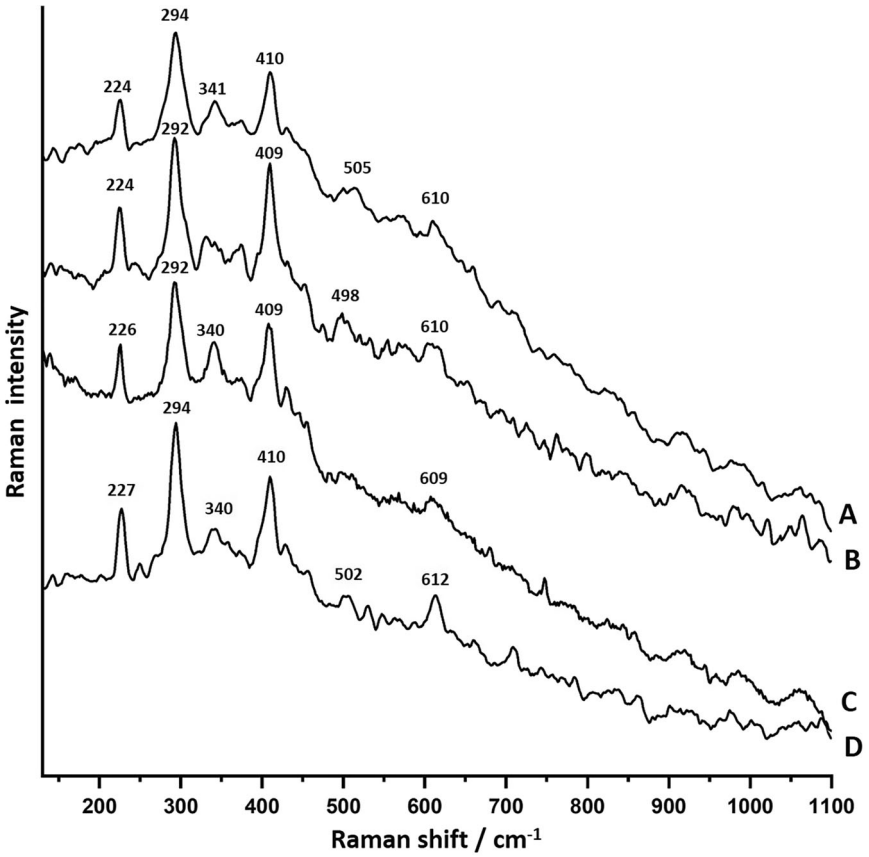

Fig. 8 | Raman spectra of haematite. A Tessera 16, type T22 (Experimental conditions: 785 nm, 300 mW, 1000 ms/acc, 40 acc.). **B** Tessera 77, type T23 (Experimental conditions: 785 nm, 300 mW, 600 ms/acc, 20 acc.). **C** Tessera 62, type E12 (Experimental conditions: 785 nm, 150 mW, 600 ms/acc, 100 acc.). **D** Tessera 39, type S7 (Experimental conditions: 785 nm, 300 mW, 600 ms/acc, 200 acc.).

For the 22 glass tesserae from the Erotes and Tethys mosaics, 13 elements were considered in the PCA, including those typically associated with chromophores and opacifiers (Al, K, Ti, Mn, Fe, Ni, Cu, Zn, Sr, Zr, Sn, Sb, Pb). The first two principal components (PC1 and PC2) accounted for 73.6% of the total variance (Fig. 9). As in the case of the stone tesserae, multiple bivariate diagrams of element pairs with diagnostic value were used to reinforce the classification described below.

Among the orange glass tesserae, sample 106 (Type E8) forms part of a larger assemblage; however, the remaining pieces were too poorly preserved and fragmented to allow for analysis. Its colour is explained by the high Cu and Pb levels recorded, which clearly distinguish it from the rest of the glass samples. The orange hue is generally attributed to the presence of cuprite (Cu_2O) crystals, while Pb is typically added to promote cuprite crystallisation and possibly enhance the glass's brilliance[10,44]. Minor amounts of Zn and Sn were also detected, suggesting the use of metalworking scraps—such as bronze or brass—as a copper source, or pewter as a source of lead[44–46].

The red tesserae 110, 111, and 112 (Type E10) also display Cu as the primary chromophore, precipitating either as metallic Cu^0 nanoparticles or

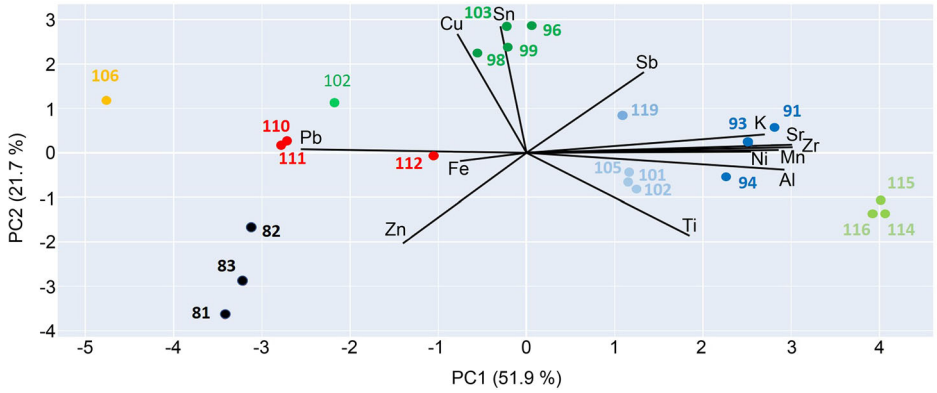

Fig. 9 | PCA results based on h-XRF data from all the glass tesserae.

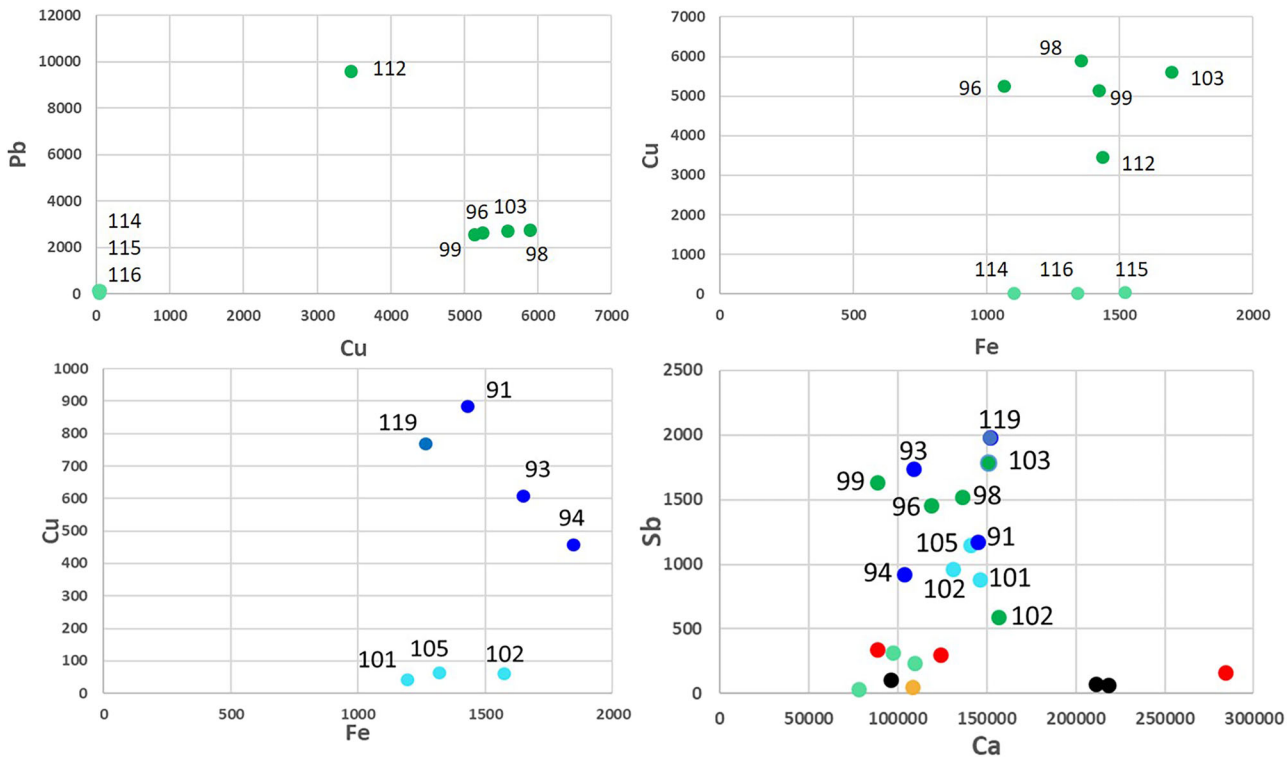

Fig. 10 | Bivariate plots (ppm) of green and blue glass tesserae and associated opacifiers. Top left: Pb vs Ca for green tesserae. Top right: Cu vs Fe for green tesserae. Bottom left: Cu vs Fe for blue tesserae. Bottom right: Sb vs Ca for all glass tesserae.

as Cu_2O crystals. This process appears to have been catalysed by the presence of elements such as Pb and Fe within the silicate matrix[47]. Iron contributes to darker tones and acts as a flux, facilitating the formation of colouring particles[48]. As observed for the orange tessera, Pb was probably added to promote cuprite crystallisation and may have favoured the growth of large dendritic Cu_2O crystals (>1 μm), producing a red hue similar to that generated by Cu^0 nanoprecipitates but under less reducing conditions[44].

The black glass tesserae 81, 82, and 83 (Type E18) contain significantly higher amounts of Fe compared with the other glass samples, suggesting that iron was responsible for the development of their black colour under reducing conditions. In such an environment, Fe shifts from its ferric (Fe^{3+}) to its ferrous (Fe^{2+}) state. Ferrous ions act as efficient chromophores, absorbing portions of the visible spectrum and causing the reflected or transmitted light to appear black[49,50]. Furthermore, the presence of S in these tesserae suggests complementarily that the darkening of the glass might also be due to the Fe-S chromophore[51].

The dark green tesserae 96, 98, and 99 (Type E22), together with sample 102 (Type T26) from the Tethys mosaic, exhibit a chromophore based on Cu^{2+}[52]. The presence of Sb in these samples suggests the use of calcium antimonate as an opacifier. Tessera 102, which contains less Cu, shows a distinct enrichment in Pb, possibly indicating the use of lead antimonate either to modulate the colour or to act as an opacifier[53] (Fig. 10).

In the light green tesserae 114, 115, and 116 (Type E23), the absence of Cu and Pb indicates that the colour can be attributed to the presence of Fe within the glassy matrix in the form of ferric oxide (Fe^{3+}) (Fig. 10). In conventional soda–lime–silicate glasses, the total iron content and a higher Fe^{2+}/Fe^{3+} ratio result in a residual greenish hue[54].

The blue tesserae 91, 93, and 94 (Type E21), 101, 102, and 105 (Type E19), as well as 119 (Type E20), form a compositional group in which the PCA distinguishes between dark and light blue varieties. The dark blue tesserae, together with sample 119, show a marked incidence of Cu, probably present as Cu^{2+} or CuO, while the intensity of their colour suggests the possible addition of cobalt. However, considering the low amount of this element necessary for colouring[55], it is likely that it was not recorded, as its concentration was below the instrument detection limit. In contrast, in the light blue tesserae, where Cu is absent, the colour can be attributed to

Table 1 | Comparison of materials identified in each mosaic

Materials	Mosaics		
	Tethys	Erotes	Scrollworks
Limestone	+++	+++	+++
Limestone + Sr	+++	+++	+++
Limestone + high Si	+	+++	+
Limestone + amorphous carbon	+++	-	+++
Marly limestone (high Si, Al, K, Fe)	+++	+	-
Ironstone	+++	+++	-
Iron-rich limestone	-	-	+++
Glass	+	+++	-

Fe^{2+} acting as the chromophore[54,56]. In all cases, as observed for the dark green tesserae, the presence of Sb and Ca indicates the use of calcium antimonate as an opacifier (Fig. 10).

Discussion

As a result of the h-Raman and h-XRF analyses, a comprehensive table of identified raw materials has been established, enabling a clearer visualization of the compositional similarities and differences among the three mosaics (Table 1). The widespread occurrence of limestone and strontium-bearing limestone suggests a shared provenance for the materials used in all three mosaics, while the varying amounts of Si point to distinct selection areas within the same geological source. The employment of ironstone tesserae in the two more intricate mosaics (Thethys and Erotes) suggests a preferential utilization of this material for more sophisticated iconographic representations; nevertheless, it must be acknowledged that a majority of the Scrollworks mosaic remains unrecovered.

The notable presence of glass tesserae and the absence of amorphous carbon-bearing limestone reinforce the distinctive character of the Erotes mosaic, likely reflecting an earlier phase of production. Unequivocally, the Erotes mosaic exhibits characteristics indicative of an intentional pursuit of enhanced luminosity, chromatic saturation, and an expanded colour palette, properties inherent to high-calibre figurative mosaic production. These preferences in the selection of materials, the compass compositional scheme, and the preserved figures (Erotes), place this mosaic in line with the Mosaico de los Amores, one of the reference mosaics in the Alto Guadalquivir[8].

Overall, the integrated archaeometric approach applied here provides new insights into the raw material procurement and technological choices underlying the manufacture of these mosaics, contributing to a more nuanced understanding of their historical and material context.

Spectroscopic analyses conducted on the three mosaics from Marroquíes Altos enabled the implementation of an effective analytical methodology, the acquisition of updated data concerning the materials employed in their manufacture, and the establishment of meaningful comparisons among them. The use of non-destructive handheld Raman and X-ray fluorescence instruments (an indispensable approach given that the mosaics are mounted on the walls of the Museum of Jaén and that no loose tesserae are available) provided reliable insights into their composition. The methodological workflow, which integrated systematic photogrammetric digitization, optimized sampling strategies, portable spectroscopy, and multivariate statistical analysis, proved both efficient and reproducible, offering a transferable model for comparable assemblages studied either in museums or in situ.

The study highlights the emerging distinctiveness of mosaics from the Upper Guadalquivir region. All three examples were produced with limestone of varied colours obtained from nearby geological formations, although specific characteristics distinguish them from one another. This is particularly evident in the Erotes mosaic, which incorporates multicoloured glass tesserae and limestone compositions that differ from those identified in the other two. Analyses of the glass tesserae indicate the deliberate application of copper-, lead-, and antimony-based formulations in accordance with glassmaking traditions widely documented during the Roman period. These results situate the Marroquíes Altos mosaics within the broader technological context of Antiquity and open new perspectives for provenance and comparative studies.

A major contribution of the research lies in the identification of ironstone within both mosaics and its selective use in specific decorative elements. When considered together with previous evidence from the Amores mosaic at Cástulo[8], this finding supports the recognition of a distinctive regional practice within the Guadalquivir mosaic school[23], setting the works from the province of Jaén apart from other Roman mosaics in Europe. Further investigation will be required to determine whether the choice of this material was primarily aesthetic or associated with symbolic or protective meanings.

Beyond the analytical outcomes, the research enhances the cultural and historical value of these mosaics as complex artefacts that embody technological knowledge, patterns of resource management, and artistic expression in Roman Hispania. By integrating archaeometric and archaeological perspectives, the study advances a comprehensive understanding of material culture in the Upper Guadalquivir area.

Data availability

All data generated or analysed during this study are included in this published article [and its supplementary information files].

Received: 29 October 2025; Accepted: 17 January 2026;
Published online: 24 January 2026

References

1. Bellón, J. P., Rueda, C., Lechuga, M. A. & Moreno, I. An Archaeological analysis of a battlefield of the Second Punic War: the camps of the battle of Baecula. *J. Rom. Archaeol.* **29**, 73–104 (2016).
2. Bellón, J. P. et al. On the location of Iliturgi: archaeological analysis of its siege in the context of the Second Punic War (in Spanish). *Arch. Esp. Arqueol.* **94**, e15 (2021).
3. Bellón, J. P., Lechuga, M. Á, Moreno, M. I. & Gutiérrez, M. Ianus Augustus, Caput Viae (Mengíbar, Spain): An interprovincial monumental border in Roman Hispania. *J. Rom. Archaeol.* **34**, 3–29 (2021).
4. Gutiérrez, M., Lechuga, M., Moreno, I. & Bellón, J. P. Microstratigraphic analysis of the main Roman road in Hispania: the Via Augusta where it passes through the Ianus Augustus (Mengíbar, Spain). *Archaeol. Anthropol. Sci.* **14**, 142 (2022).
5. Boschetti, C., Henderson, J., Evans, J. & Leonelli, C. Mosaic tesserae from Italy and the production of Mediterranean coloured glass (4rd century BCE–4th century CE). Part I: Chemical composition and technology. *J. Archaeol. Sci. Rep.* **7**, 303–311 (2016).
6. Casas, L. et al. The Colours of the Circus Mosaic from Barcino (Roman Barcelona): Characterization, Provenance, and Technology Issues. *Minerals* **11**, 746 (2021).
7. Di Bella, M., Quartieri, S., Sabatino, G., Santalucia, F. & Triscar, M. The glass mosaics tesserae of "Villa del Casale" (Piazza Armerina, Italy): a multi-technique archaeometric study. *Archaeol. Anthropol. Sci.* **6**, 345–362 (2014).
8. Sánchez, A. et al. First insights into the archaeometric analysis of the Los Amores Mosaic in Cástulo (Linares, Spain): the Judgement of Paris. *Herit. Sci.* **9**, 8 (2021).
9. Maltoni, S. & Silvestri, A. Mosaic of colours: investigating production technologies of Roman glass tesserae from Northeastern Italy. *Minerals* **8**, 255 (2018).
10. Schibille, N., Boschetti, N. C., Valero, M. A., Veron, E. & de Juan, J. The colour palette of the mosaics in the Roman villa of Noheda (Spain). *Minerals* **10**, 272 (2020).
11. Fiorenza, E. et al. Vitreous tesserae from the Four Seasons Mosaic of the S. Aloe Quarter in Vibo Valentia–Calabria, Italy: A Chemical Characterization. *Minerals* **10**, 658 (2020).

12. Miletić, S. et al. Identification and provenance determination of stone tesserae used in mosaics from Roman Celeia, Slovenia. *Archaeometry* **64**, 561–577 (2022).
13. Marcaida, I. et al. *In situ* non-invasive multianalytical methodology to characterize mosaic tesserae from the House of Gilded Cupids, Pompeii. *Herit. Sci.* **7**, 9 (2019).
14. Balassone, G. et al. From tiny to immense: Geological spotlight on the Alexander Mosaic (National Archaeological Museum of Naples, Italy) using non-invasive in situ analyses. *PLoS ONE* **20**, e0315188 (2025).
15. Palomar, T., Garcia-Heras, M., Saiz-Jimenez, C., Márquez, C. & Villegas, M. A. Pathologies and analytical study of mosaic materials from Carmona and Italica. *Mater. Constr,* **61**, 629–636 (2011).
16. Colantonio, C., Baldassarri, P., Avino, P., Astolfi, M. L. & Visco, G. Degradation of the black and white mosaic of a *Roman domus* under Palazzo Valentini in Rome: A Preliminary Study. *Molecules* **27**, 765 (2022).
17. Espantaleón, R. New findings at Marroquíes Altos (in Spanish). *Bol. Instit. Est. Gien*. 10/1960-12/1960. (1960).
18. Fernández, D. Hispanic mosaics with compass-based geometric schemes (in Spanish). (Gráficas J.C.J. 1980).
19. Blázquez, J. M. Roman mosaics of Córdoba, Jaén, and Málaga (in Spanish). (Consejo Superior de Investigaciones Científicas, 1981).
20. San Nicolás, Mª. P. Mythological beings and allegorical figures in Roman mosaics of Hispania in relation to water (in Spanish). *Espacio, Tiempo y Forma, Serie II, Historia Antigua* **17-18**, 301–333; https://doi.org/10.5944/etfii.17-18.2004 (2004–2005).
21. Sánchez, A. et al. Raman analysis of Roman mosaics from the Upper Guadalquivir Valley (Spain). *J. Raman Spectrosc.* **56**, 1279–1289 (2025).
22. San Nicolas, Mª. P. Iconographic interrelation of Thetys and Thalassa in Hispano-Roman mosaics (in Spanish). *Espac*. *Tiempo y Forma. Ser. I, Prehi. y Arqueol*. **1**, 315–320; https://doi.org/10.5944/etfi.1.2008.1930 (2008).
23. San Nicolás, Mª. P. A mosaic workshop in Jaén (Spain) (in Spanish). *Espac*. *Tiempo Forma, Ser. II Hist. Antig*. **31**, 113-120; https://doi.org/10.5944/etfii.31.2018.22658 (2018).
24. Colomban, P. The on-site/remote Raman analysis with mobile instruments: a review of drawbacks and success in cultural heritage studies and other associated fields. *J. Raman Spectrosc.* **43**, 1529–1535 (2012).
25. Rousaki, A. & Vandenabeele, P. In situ Raman spectroscopy for cultural heritage studies. *J. Raman. Spectrosc.* **52**, 2178 (2021).
26. Solé, V. A., Papillon, E. M., Cotte, M., Walter, P. & Susini, J. A multiplatform code for the analysis of energy-dispersive X-ray fluorescence spectra. *Spectrochim. Acta Part B* **62**, 63–68 (2007).
27. Yatsuk, O. et al. Data from multiple portable XRF units and their significance for ancient glass studies. *Molecules* **27**, 6068 (2022).
28. Bartolozzi, G. et al. Mosaic Tesserae from the Roman Villa of Aiano in Tuscany (Italy): Characterization via a Non-Invasive Protocol. *Heritage* **8**, 290 (2025).
29. Gunasekaran, S., Anbalagan, G. & Pandi, S. Raman and infrared spectra of carbonates of calcite structure. *J. Raman Spectrosc.* **37**, 892–899 (2006).
30. Sun, J., Wu, Z. Cheng, H. Zhang, Z. & Frost, R. L. *Spectrochim. Acta. A Mol. Biomol. Spectrosc*.**117**, 158; https://doi.org/10.1016/j.saa.2013.08.014 (2014).
31. Yonghwi Kim, Y., Caumon, M.-C., Barres, O., Sall, A. & Cauzid, J. Identification and composition of carbonate minerals of the calcite structure by Raman and infrared spectroscopies using portable devices. *Spectrochim. Acta A Mol. Biomol. Spectrosc.* **261**, 119980 (2021).
32. Bersani, D. & Lottici, P. P. Raman spectroscopy of minerals and mineral pigments in archaeometry. *J. Raman Spectrosc.* **47**, 499–530 (2016).
33. Murphy, A. E., Jakubek, R. S., Steele, A., Fries, M. D. & Glamoclija, M. Raman spectroscopy provides insight into carbonate rock fabric based on calcite and dolomite crystal orientation. *J. Raman Spectrosc.* **52**, 1155–1166 (2021).
34. Raneri, S. et al. Raman spectroscopy as a tool for provenancing black limestones (bigi morati) used in Antiquity. *J. Raman Spectrosc.* **52**, 241–250 (2021).
35. Yuan, R. uichuan et al. Raman spectroscopy analysis of disordered and amorphous carbon materials: A review of empirical correlations. *Carbon* **238**, 120214 (2025).
36. Abad, Mª I. & Molina, J. M. (2012): Minerals and rocks of the province of Jaén (in Spanish). (Universidad de Jaén, 2012).
37. Luna, J. V. Tessellated mosaics in the Roman world: the House of Bacchus from the perspective of a mosaicist (in Spanish). *Rev. Electr. ReCoPaR* **10**, 1–43 (2013).
38. de Faria, D. L. A. & Lopes, F. N. Heated goethite and natural hematite: Can Raman spectroscopy be used to differentiate them?. *Vib. Spectrosc.* **45**, 117–121 (2007).
39. Hanesch, M. Raman spectroscopy of iron oxides and (oxy)hydroxides at low laser power and possible applications in environmental magnetic studies. *Geophys. J. Int.* **177**, 941–948 (2009).
40. Marshall, C. P., Dufresne, W. J. B. & Rufledt, C. J. Polarized Raman spectra of hematite and assignment of external modes. *J. Raman Spectrosc.* **51**, 1522–1529 (2020).
41. Petit, M.ªD., Rucandio, M.ªI., Galan, A. & Garcia, R. Usefulness of geological, mineralogical, chemical and chemometric analytical techniques in exploitation and profitability studies of iron mines and their associated elements. *J. Geochem. Explor.* **98**, 116–128 (2008).
42. Ji, Z. et al. Microstructure and Minerals Evolution of Iron Ore Sinter: Influence of SiO_2 and Al_2O_3. *Minerals* **9**, 449 (2019).
43. Parras, D. et al. Micro-Raman spectroscopy of decorated pottery from the Iberian archaeological site of Puente Tablas (Jaén, Spain, 7th–4th century B.C.). *J. Raman Spectrosc.* **41**, 68–73 (2010).
44. Noirot, C. et al. Comparative Investigation of Red and Orange Roman Tesserae: Role of Cu and Pb in Colour Formation. *Heritage* **5**, 2628–2645 (2022).
45. Fiori, C. Production technology of Byzantine red mosaic glasses. *Ceram. Int.* **41**, 3152–3157 (2015).
46. Barca, D. et al. Vitreous tesserae from the calidarium mosaics of the Villa dei Quintili, Rome. Chemical composition and production technology. *Microchem. J.* **124**, 726–735 (2016).
47. Bandiera, M. et al. Nanotechnology in Roman opaque red glass from the 2nd century AD. Archaeometric investigation in red sectilia from the decoration of the Lucius Verus Villa in Rome. *Heritage* **2**, 2597–2611 (2019).
48. Ricciardi, P., Colomban, P., Tournié, A., Macchiarola, M. & Ayed, N. A non-invasive study of Roman Age mosaic glass tesserae by means of Raman spectroscopy. *J. Archaeol. Sci.* **36**, 2551–2559 (2009).
49. Ceglia, A. et al. A XANES study of chromophores: the case of black glass. *Anal. Methods* **6**, 2662–2671 (2014).
50. Cagno, S. et al. Deeply colored and black-appearing Roman glass: a continued research. *J. Archaeol. Sci.* **42**, 128–139 (2014).
51. Maltoni, S. & Silvestri, A. Mosaic of Colors: investigating production technologies of Roman Glass Tesserae from Northeastern Italy. *Minerals* **8**, 255 (2018).
52. L. C. Prinsloo, L. C. & Colomban, P. A Raman spectroscopic study of the Mapungubwe oblates: glass trade beads excavated at an Iron Age archaeological site in South Africa. *J. Raman Spectrosc*. **39**, 79–90; https://doi.org/10.1002/jrs.1816 (2008).
53. Basson, E. et al. Characterization of colorants and opacifiers in Roman glass mosaic tesserae through spectroscopic and spectrometric techniques. *J. Raman Spectrosc.* **45**, 238–245 (2014).
54. García-Heras, M., Rincón, J. M. ª, Jimeno, A. & Villegas, M. A. Pre-Roman coloured glass beads from the Iberian Peninsula: a chemico-physical characterisation study. *J. Archaeol. Sci.* **32**, 727–738 (2005).
55. Gedzevičiūtė, V., Welter, N., Schüssler, U. & Weiss, C. Chemical composition and colouring agents of Roman mosaic and millefiori

glass, studied by electron microprobe analysis and Raman microspectroscopy. *Archaeol. Anthr. Sci.* **1**, 15–29 (2009).
56. Donald, S. B., Swink, A. M. & Schreiber, H. D. High-iron ferric glass. *J. Non-Cryst. Solids* **352**, 539–543 (2006).

Acknowledgements

This study was funded by GeoChemMos project, Junta de Andalucía, Consejería de Universidad, Investigación e Innovación (PAIDI2020). Convocatoria 2021. Proyectos de investigación orientados a los retos de la Sociedad, ProyExcel_00269. The funder playedno role in study design, data collection, analysis and interpretation of data, or the writing of this manuscript.

Author contributions

A.S.: Investigation, Conceptualization, Methodology, Writing–original draft. M.M. Methodology, Investigation, h-Raman analysis. J.T.: Methodology, Investigation, h-Raman analysis. P.V.: Methodology, h-XRF analysis. P.T.: Methodology, h-XRF analysis, S.V.: h-XRF analysis, T.R.: h-XRF analysis. All authors read and approved the final manuscript.

Competing interests

The authors declare no competing interests.

Additional information

Supplementary information The online version contains supplementary material available at https://doi.org/10.1038/s40494-026-02339-4.

Correspondence and requests for materials should be addressed to Alberto Sánchez.